JOURNAL OF COMPUTATIONAL PHYSICS **139,** 327–342 (1998)
ARTICLE NO. CP975881

Nonreflecting Boundary Conditions for Maxwell's Equations

Marcus J. Grote*,[1] and Joseph B. Keller†,[2]

*Courant Institute of Mathematical Sciences, New York University, New York, New York 10012; †Departments of Mathematics and Mechanical Engineering, Stanford University, Stanford, California 94305-2125
E-mail: grote@cims.nyu.edu, keller@math.stanford.edu

Received July 22, 1996; revised June 27, 1997

Exact nonreflecting boundary conditions are derived for the time dependent Maxwell equations in three space dimensions. These conditions hold on a spherical surface $\mathcal{B}$, outside of which the medium is assumed to be homogeneous, isotropic, and source-free. They are local in time and nonlocal on $\mathcal{B}$, and they do not involve high-order derivatives. Thus, they are easy to incorporate into finite difference or finite element methods. These boundary conditions are similar to the exact nonreflecting boundary conditions for the scalar wave equation which yield high numerical accuracy.

1. INTRODUCTION

We consider electromagnetic scattering in unbounded three-dimensional space. The scattering region may contain obstacles, inhomogeneities, and nonlinearities. To treat it numerically we surround the region of interest by an artificial boundary $\mathcal{B}$, and we denote by Ω the computational domain inside $\mathcal{B}$. At $\mathcal{B}$ we impose an exact nonreflecting boundary condition upon the scattered field. This condition is local in time but nonlocal on $\mathcal{B}$. It is the extension to Maxwell's equations of the exact nonreflecting boundary condition which we have derived for the scalar wave equation [1]. We have shown [2] that it yields high accuracy in numerical computations.

Usually various approximate boundary conditions are used, which are local differential operators on $\mathcal{B}$. Examples are the Mur [3] and the Peterson [4] conditions, which are the generalizations to Maxwell's equations of the absorbing boundary conditions derived for the scalar wave equation by Engquist and Majda [5] and by Bayliss and Turkel [6]. A different approach has been to add an artificial absorbing layer outside $\mathcal{B}$, which is supposed to

[1] This work was supported by an IBM fellowship and NSF Grant DMS-9596102.
[2] This work was supported in part by the AFOSR, NSF, and ONR.

0021-9991/98 $25.00

absorb outgoing waves [7]. Neither of these approaches leads to complete absorption of waves at all angles of incidence. To minimize the amount of reflection and to achieve very high accuracy, it is often necessary to move $\mathcal{B}$ far from the region of interest, or to use a thick absorbing layer. Both procedures are expensive in computer storage and execution time. Moreover, with limited memory it may not be possible to achieve a desired accuracy.

For the time-dependent scalar wave equation, Lindman [8] devised a boundary condition for use on a plane boundary. Randall [9] adapted it to the elastic wave equation. It requires solving the inhomogeneous wave equation on the boundary a number of times.

An exact nonreflecting boundary condition for the wave equation was proposed by Ting and Miksis [10]. It is based on a Kirchhoff integral representation of the solution outside $\mathcal{B}$, and it was generalized to Maxwell's equations by De Moerloose and De Zutter [11]. Since this boundary condition requires storing the solution at $\mathcal{B}$ for the amount of time it takes a wave to propagate across Ω, this approach is expensive in both storage and computer resources.

It is to avoid these difficulties that we have developed this new boundary condition for the special case when $\mathcal{B}$ is a sphere. It is derived in Section 2. In Section 3, we show how to combine it with the finite difference method. Then in Section 4, we derive alternative formulations, which are useful when the vector wave equation or the weak form of Maxwell's equations is used. In Section 5, we discuss higher order boundary conditions, and finally in Section 6, we present numerical results which demonstrate the high accuracy of our boundary condition.

2. DERIVATION OF THE BOUNDARY CONDITIONS

We choose $\mathcal{B}$ to be a sphere of radius R. In $\mathcal{B}^{ext}$, the region outside $\mathcal{B}$, the medium is assumed to be linear, homogeneous, isotropic, of constant electric permittivity ε, of constant magnetic permeability μ, and of zero conductivity. In addition, we assume that at $t = 0$ the scattered field is confined to the computational domain Ω. In $\mathcal{B}^{ext}$ the electric field $\boldsymbol{E}$ and the magnetic field $\boldsymbol{H}$ satisfy Maxwell's equations

$$\nabla \times \boldsymbol{H} = \varepsilon \frac{\partial \boldsymbol{E}}{\partial t}, \quad \nabla \times \boldsymbol{E} = -\mu \frac{\partial \boldsymbol{H}}{\partial t}. \tag{2.1}$$

Both $\boldsymbol{E}$ and $\boldsymbol{H}$ vanish at $t = 0$ in $\mathcal{B}^{ext}$, so $\nabla \cdot \boldsymbol{E} = \nabla \cdot \boldsymbol{H} = 0$ at $t = 0$. From (2.1) it follows that they remain solenoidal there for all time:

$$\nabla \cdot \boldsymbol{E} = \nabla \cdot \boldsymbol{H} = 0. \tag{2.2}$$

From (2.1) it also follows that both $\boldsymbol{E}$ and $\boldsymbol{H}$ satisfy the vector wave equation in $\mathcal{B}^{ext}$:

$$\frac{1}{c^2}\frac{\partial^2 \boldsymbol{E}}{\partial t^2} + \nabla \times \nabla \times \boldsymbol{E} = 0, \quad \frac{1}{c^2}\frac{\partial^2 \boldsymbol{H}}{\partial t^2} + \nabla \times \nabla \times \boldsymbol{H} = 0. \tag{2.3}$$

Here $c = 1/\sqrt{\varepsilon\mu}$.

We introduce the polar coordinates $r,\ \vartheta,\ \phi$ and the unit vectors $\hat{\boldsymbol{r}}, \hat{\boldsymbol{\vartheta}}, \hat{\boldsymbol{\phi}}$. Next, we let Y_{nm} denote the nmth spherical harmonic

$$Y_{nm}(\vartheta, \phi) = \sqrt{\frac{(2n+1)(n-|m|)!}{4\pi(n+|m|)!}} P_n^{|m|}(\cos\vartheta) e^{im\phi}, \quad n \geq 0,\ |m| \leq n. \tag{2.4}$$

The Y_{nm} are orthonormal with respect to the L_2 inner product on the *unit* sphere. If the problem considered is real, it is advantageous to use the real spherical harmonics, given by the real and imaginary parts of (2.4) with a modified normalization constant.

Following [12, p. 170], we let $\boldsymbol{U}_{nm}$ and $\boldsymbol{V}_{nm}$ denote the vector spherical harmonics

$$\boldsymbol{U}_{nm}(\vartheta,\phi) = \frac{r\nabla Y_{nm}}{\sqrt{n(n+1)}} = \frac{1}{\sqrt{n(n+1)}}\left[\frac{\partial Y_{nm}}{\partial\vartheta}\hat{\boldsymbol{\vartheta}} + \frac{1}{\sin\vartheta}\frac{\partial Y_{nm}}{\partial\phi}\hat{\boldsymbol{\phi}}\right], \tag{2.5}$$

$$\boldsymbol{V}_{nm}(\vartheta,\phi) = \hat{\boldsymbol{r}}\times\boldsymbol{U}_{nm} = \frac{1}{\sqrt{n(n+1)}}\left[\frac{-1}{\sin\vartheta}\frac{\partial Y_{nm}}{\partial\phi}\hat{\boldsymbol{\vartheta}} + \frac{\partial Y_{nm}}{\partial\vartheta}\hat{\boldsymbol{\phi}}\right]. \tag{2.6}$$

They form an orthonormal basis for the space of tangential L_2 fields on the unit sphere with respect to the L_2 inner product [12]. They also satisfy the following useful equations for any $f(r)$:

$$\nabla\times(f(r)\boldsymbol{V}_{nm}) = -\frac{\sqrt{n(n+1)}\,f(r)}{r}Y_{nm}\hat{\boldsymbol{r}} - \frac{1}{r}\frac{\partial(rf(r))}{\partial r}\boldsymbol{U}_{nm}, \tag{2.7}$$

$$\hat{\boldsymbol{r}}\times\nabla\times(f(r)\boldsymbol{V}_{nm}) = -\frac{1}{r}\frac{\partial(rf(r))}{\partial r}\boldsymbol{V}_{nm}. \tag{2.8}$$

To solve (2.1) in $\mathcal{B}^{ext}$, we decompose the electromagnetic field into transverse electric (TE) and transverse magnetic (TM) fields. The electric component of the TE multipole field of order (n,m) is given by

$$\boldsymbol{E}^{\mathrm{TE}}_{nm}(r,\vartheta,\phi,t) = f_{nm}(r,t)\boldsymbol{V}_{nm}(\vartheta,\phi), \tag{2.9}$$

where f_{nm} satisfies

$$L_n[f_{nm}] \equiv \left(\frac{1}{c^2}\frac{\partial^2}{\partial t^2} - \frac{\partial^2}{\partial r^2} - \frac{2}{r}\frac{\partial}{\partial r} + \frac{n(n+1)}{r^2}\right)f_{nm} = 0. \tag{2.10}$$

The magnetic component of the TM multipole field of order (n,m) is given by

$$\boldsymbol{H}^{\mathrm{TM}}_{nm}(r,\vartheta,\phi,t) = g_{nm}(r,t)\boldsymbol{V}_{nm}(\vartheta,\phi), \tag{2.11}$$

where $L_n[g_{nm}] = 0$.

The TE and TM solutions form a complete set of solutions of Maxwell's equations in a source-free region [13, p. 746]. Therefore, the general electric and magnetic multipole fields of order (n,m) are obtained by combining (2.9) with the electric field associated with (2.11), and combining (2.11) with the magnetic field associated with (2.9), respectively:

$$\boldsymbol{E}_{nm}(r,\vartheta,\phi,t) = f_{nm}(r,t)\boldsymbol{V}_{nm} + \frac{1}{\varepsilon}\nabla\times\left[\boldsymbol{V}_{nm}\int_0^t g_{nm}(r,s)\,ds\right], \tag{2.12}$$

$$\boldsymbol{H}_{nm}(r,\vartheta,\phi,t) = -\frac{1}{\mu}\nabla\times\left[\boldsymbol{V}_{nm}\int_0^t f_{nm}(r,s)\,ds\right] + g_{nm}(r,t)\boldsymbol{V}_{nm}. \tag{2.13}$$

In $\mathcal{B}^{ext}$, the total electromagnetic field is a superposition of multipole fields:

$$\boldsymbol{E} = \sum_{n\geq 1}\sum_{|m|\leq n}\boldsymbol{E}_{nm}, \quad \boldsymbol{H} = \sum_{n\geq 1}\sum_{|m|\leq n}\boldsymbol{H}_{nm}. \tag{2.14}$$

By using (2.7) we see that the terms in (2.12) and (2.13) that involve $\nabla \times (\boldsymbol{V}_{nm} \cdots)$ are orthogonal to $\boldsymbol{V}_{nm}$. Thus from (2.14) we conclude that

$$f_{nm} = (\boldsymbol{E}, \boldsymbol{V}_{nm}), \quad g_{nm} = (\boldsymbol{H}, \boldsymbol{V}_{nm}). \tag{2.15}$$

The inner product involves integration with respect to ϑ and ϕ on the sphere of radius r.

To obtain a boundary condition for $\boldsymbol{H}_{nm}$, we first apply $\hat{\boldsymbol{r}} \times \nabla \times$ to (2.13). We use (2.8) and the fact that $\boldsymbol{V}_{nm} \int_0^t f_{nm}$ is also a solution of (2.3) to get

$$\hat{\boldsymbol{r}} \times \nabla \times \boldsymbol{H}_{nm} = -\sqrt{\frac{\varepsilon}{\mu}} \frac{1}{c} \frac{\partial f_{nm}}{\partial t} \boldsymbol{U}_{nm} - \frac{1}{r} \frac{\partial (r g_{nm})}{\partial r} \boldsymbol{V}_{nm}. \tag{2.16}$$

Next we differentiate (2.13) with respect to t and simplify the result using (2.7). The tangential components of the resulting equation yield

$$\frac{1}{c} \frac{\partial \boldsymbol{H}_{nm}^{\tan}}{\partial t} = \sqrt{\frac{\varepsilon}{\mu}} \frac{1}{r} \frac{\partial (r f_{nm})}{\partial r} \boldsymbol{U}_{nm} + \frac{1}{c} \frac{\partial g_{nm}}{\partial t} \boldsymbol{V}_{nm}. \tag{2.17}$$

Now we subtract (2.17) from (2.16) to get

$$\begin{aligned} \hat{\boldsymbol{r}} \times \nabla \times \boldsymbol{H}_{nm} - \frac{1}{c} \frac{\partial \boldsymbol{H}_{nm}^{\tan}}{\partial t} = &-\sqrt{\frac{\varepsilon}{\mu}} \frac{1}{r} \left(\frac{\partial}{\partial r} + \frac{1}{c} \frac{\partial}{\partial t} \right) [r f_{nm}] \boldsymbol{U}_{nm} \\ &- \frac{1}{r} \left(\frac{\partial}{\partial r} + \frac{1}{c} \frac{\partial}{\partial t} \right) [r g_{nm}] \boldsymbol{V}_{nm}. \end{aligned} \tag{2.18}$$

Similarly from (2.12) we derive the equation

$$\begin{aligned} \hat{\boldsymbol{r}} \times \nabla \times \boldsymbol{E}_{nm} - \frac{1}{c} \frac{\partial \boldsymbol{E}_{nm}^{\tan}}{\partial t} = &-\frac{1}{r} \left(\frac{\partial}{\partial r} + \frac{1}{c} \frac{\partial}{\partial t} \right) [r f_{nm}] \boldsymbol{V}_{nm} \\ &+ \sqrt{\frac{\mu}{\varepsilon}} \frac{1}{r} \left(\frac{\partial}{\partial r} + \frac{1}{c} \frac{\partial}{\partial t} \right) [r g_{nm}] \boldsymbol{U}_{nm}. \end{aligned} \tag{2.19}$$

Equations (2.18) and (2.19) cannot yet be used as boundary conditions because their right-hand sides involve radial derivatives of the unknown functions f_{nm} and g_{nm}. To eliminate these derivatives we note that f_{nm} and g_{nm} satisfy the differential equation (2.10) and that they both vanish at $t = 0$ for $r \geq R$. Equation (2.10) is the equation satisfied by the coefficient of Y_{nm} in the expansion of a solution of the scalar wave equation. Therefore at $r = R$, f_{nm} satisfies the following boundary condition, which was derived in [1] for the wave equation and used in [2]:

$$\left(\frac{\partial}{\partial r} + \frac{1}{c} \frac{\partial}{\partial t} \right) [r f_{nm}] = -\boldsymbol{d}_n \cdot \boldsymbol{\psi}_{nm}^E(t), \quad r = R. \tag{2.20}$$

This is the nmth component of (2.6) in [2] with $\boldsymbol{c} = \boldsymbol{d}$ and $\boldsymbol{z} = \boldsymbol{\psi}$. Here $\boldsymbol{d}$ and $\boldsymbol{\psi}$ are n component vectors.

The vector function $\boldsymbol{\psi}_{nm}^E(t) = \{\psi_{nm}^{E,j}(t)\}$, $j = 1, \ldots, n$, satisfies the *linear first-order ordinary* differential equation

$$\frac{1}{c} \frac{d}{dt} \boldsymbol{\psi}_{nm}^E(t) = \boldsymbol{A}_n \boldsymbol{\psi}_{nm}^E(t) + f_{nm}(R, t) \boldsymbol{e}_n, \quad \boldsymbol{\psi}_{nm}^E(0) = 0. \tag{2.21}$$

Here $\boldsymbol{A}_n = \{A_n^{ij}\}$ is the constant $n \times n$ matrix

$$A_n^{ij} = \begin{cases} -n(n+1)/(2R^j) & \text{if } i = 1, \\ (n+i)(n+1-i)/(2i) & \text{if } i = j+1, \\ 0 & \text{otherwise.} \end{cases} \tag{2.22}$$

The constant n-component vectors $\boldsymbol{d}_n = \{d_n^j\}$ and $\boldsymbol{e}_n = \{e_n^j\}$ are defined as

$$d_n^j = \frac{n(n+1)j}{2R^j}, \quad j = 1, \ldots, n, \tag{2.23}$$

$$\boldsymbol{e}_n = [1, 0, \ldots, 0]^\top. \tag{2.24}$$

Since $L_n[g_{nm}] = 0$, we also have

$$\left(\frac{\partial}{\partial r} + \frac{1}{c}\frac{\partial}{\partial t}\right)[r g_{nm}] = -\boldsymbol{d}_n \cdot \boldsymbol{\psi}_{nm}^H(t), \quad r = R, \tag{2.25}$$

where the n-component vector function $\boldsymbol{\psi}_{nm}^H(t)$ satisfies the ordinary differential equation

$$\frac{1}{c}\frac{d}{dt}\boldsymbol{\psi}_{nm}^H(t) = \boldsymbol{A}_n \boldsymbol{\psi}_{nm}^H(t) + g_{nm}(R,t)\boldsymbol{e}_n, \quad \boldsymbol{\psi}_{nm}^H(0) = 0. \tag{2.26}$$

Now, we use (2.20) and (2.25) to eliminate the radial derivatives of f_{nm} and g_{nm} from (2.18) and (2.19). Thus we rewrite (2.18) and (2.19) at $r = R$ as

$$\hat{\boldsymbol{r}} \times \nabla \times \boldsymbol{H}_{nm} - \frac{1}{c}\frac{\partial \boldsymbol{H}_{nm}^{\tan}}{\partial t} = \sqrt{\frac{\varepsilon}{\mu}}\frac{1}{R}\boldsymbol{d}_n \cdot \boldsymbol{\psi}_{nm}^E(t)\boldsymbol{U}_{nm} + \frac{1}{R}\boldsymbol{d}_n \cdot \boldsymbol{\psi}_{nm}^H(t)\boldsymbol{V}_{nm}, \quad r = R, \tag{2.27}$$

$$\hat{\boldsymbol{r}} \times \nabla \times \boldsymbol{E}_{nm} - \frac{1}{c}\frac{\partial \boldsymbol{E}_{nm}^{\tan}}{\partial t} = \frac{1}{R}\boldsymbol{d}_n \cdot \boldsymbol{\psi}_{nm}^E(t)\boldsymbol{V}_{nm} - \sqrt{\frac{\mu}{\varepsilon}}\frac{1}{R}\boldsymbol{d}_n \cdot \boldsymbol{\psi}_{nm}^H(t)\boldsymbol{U}_{nm}, \quad r = R. \tag{2.28}$$

Finally, we obtain the boundary condition at $r = R$ by summing over n and m in (2.27) and (2.28):

$$\hat{\boldsymbol{r}} \times \nabla \times \boldsymbol{H} - \frac{1}{c}\frac{\partial \boldsymbol{H}^{\tan}}{\partial t} = \sqrt{\frac{\varepsilon}{\mu}}\frac{1}{R}\sum_{n\geq 1}\sum_{|m|\leq n}\boldsymbol{d}_n \cdot \boldsymbol{\psi}_{nm}^E(t)\boldsymbol{U}_{nm} + \frac{1}{R}\sum_{n\geq 1}\sum_{|m|\leq n}\boldsymbol{d}_n \cdot \boldsymbol{\psi}_{nm}^H(t)\boldsymbol{V}_{nm}, \quad r = R, \tag{2.29}$$

$$\hat{\boldsymbol{r}} \times \nabla \times \boldsymbol{E} - \frac{1}{c}\frac{\partial \boldsymbol{E}^{\tan}}{\partial t} = \frac{1}{R}\sum_{n\geq 1}\sum_{|m|\leq n}\boldsymbol{d}_n \cdot \boldsymbol{\psi}_{nm}^E(t)\boldsymbol{V}_{nm} - \sqrt{\frac{\mu}{\varepsilon}}\frac{1}{R}\sum_{n\geq 1}\sum_{|m|\leq n}\boldsymbol{d}_n \cdot \boldsymbol{\psi}_{nm}^H(t)\boldsymbol{U}_{nm}, \quad r = R. \tag{2.30}$$

The vector functions $\psi^E_{nm}(t)$ and $\psi^H_{nm}(t)$ in (2.29) and (2.30) satisfy the linear ordinary differential equations (2.21) and (2.26), which can be written as follows by using (2.15):

$$\frac{1}{c}\frac{d}{dt}\psi^E_{nm}(t) = \boldsymbol{A}_n\psi^E_{nm}(t) + (\boldsymbol{E}^{\tan}|_{r=R}, \boldsymbol{V}_{nm})\boldsymbol{e}_n, \quad \psi^E_{nm}(0) = 0. \tag{2.31}$$

$$\frac{1}{c}\frac{d}{dt}\psi^H_{nm}(t) = \boldsymbol{A}_n\psi^H_{nm}(t) + (\boldsymbol{H}^{\tan}|_{r=R}, \boldsymbol{V}_{nm})\boldsymbol{e}_n, \quad \psi^H_{nm}(0) = 0. \tag{2.32}$$

Each inner product in (2.31) and (2.32) involves two, not three, scalar inner products since $\boldsymbol{V}_{nm}$ is purely tangential. Equations (2.29) and (2.30) are the boundary conditions which we sought. They are exact and ensure that no spurious reflections occur at $\mathcal{B}$. They involve only first-order derivatives and can be incorporated easily into numerical methods.

The functions f_{nm} and g_{nm} satisfy the scalar wave equation and determine the electromagnetic field uniquely outside $\mathcal{B}$. It was shown in [2] that for smooth solutions of the scalar wave equation, imposing the exact boundary condition at $\mathcal{B}$ guarantees that the solution in Ω coincides with the restriction to Ω of the solution to the Cauchy problem in the unbounded domain. Therefore for smooth data, the solution to the initial boundary value problem inside Ω with (2.29) or (2.30) imposed at $\mathcal{B}$ is unique and coincides with the restriction to Ω of the electromagnetic field in the unbounded domain. It is also well posed with respect to perturbations in the initial conditions.

These boundary conditions do not require saving past values of $\boldsymbol{E}$ or $\boldsymbol{H}$. Instead they involve the two functions $\psi^E_{nm}(t)$ and $\psi^H_{nm}(t)$. The amount of memory needed to store them, about $(4/3)N^3$ scalar values, is negligible when compared to the storage required for $\boldsymbol{E}$ and $\boldsymbol{H}$. Most of the extra work involved in applying the boundary condition results from computing the inner products of $\boldsymbol{E}$ and $\boldsymbol{H}$ with $\boldsymbol{V}_{nm}$ in (2.31) and (2.32) and from computing the right-hand sides of (2.29) and (2.30).

To compute the Fourier components in (2.29) or (2.30), it is not necessary to compute $O(N^2)$ inner products over the entire sphere. Indeed, since the vector spherical harmonics $\boldsymbol{V}_{nm}$ separate in θ and ϕ, it is sufficient to compute $O(N)$ inner products with $\cos(m\phi)$ and $\sin(m\phi)$ over the sphere and then to compute $O(N^2)$ *one-dimensional* inner products in θ over $[0, \pi]$. The same trick can be used to calculate the sums over n and m on the right of (2.29) and (2.30).

3. THE FINITE DIFFERENCE METHOD

We shall now show how the nonreflecting boundary condition fits into the finite difference time domain method (FDTD). First proposed by Yee [14], this popular method staggers both $\boldsymbol{E}$ and $\boldsymbol{H}$ in time and space and thereby achieves second-order accuracy using current values only. Due to the nature of the Yee scheme, the boundary condition is needed only for one of the two electromagnetic field components. We choose to apply it to $\boldsymbol{E}$. Thus $\boldsymbol{E}^{\tan}$ is known at $r = R - \Delta r$ and $r = R$, whereas $\boldsymbol{H}^{\tan}$ is known at $r = R - \Delta r/2$. The boundary condition is necessary to advance $\boldsymbol{E}^{\tan}$ at $r = R$, since Maxwell's equations (2.1) would require radial derivatives of $H^{\tan}$, whose finite difference approximation involves unknown values of $\boldsymbol{H}^{\tan}$ outside $\mathcal{B}$. Thus we shall use (2.30) to advance $\boldsymbol{E}^{\tan}$ at $r = R$ from time t to time $t + \Delta t$. To do so, we apply (2.30) at $t = t + \Delta t/2$ and $r = R - \Delta r/2$, and approximate the first-order derivatives on the left by centered finite differences [15, Section 3.7].

The right side of (2.30) involves infinite sums which are truncated at a finite value N. It requires the values of $\psi^E_{nm}(t)$ and $\psi^H_{nm}(t)$ at $t = t + \Delta t/2$. These are computed concurrently with the solution inside Ω, using the linear ordinary differential equations (2.31) and (2.32). The inner products in (2.31) and (2.32) are computed over the sphere $r = R - \Delta r/2$ using the fourth-order Simpson rule. To solve (2.31) and (2.32) numerically, we opt for the trapezoidal rule [16, Sec. II.7], because the eigenvalues of the matrices $\boldsymbol{A}_n$ lie in the left half of the complex plane [2]. Since the trapezoidal rule is unconditionally stable, there is no restriction on the time-step in the integration of (2.31) and (2.32). The work required in solving the linear systems (2.31) and (2.32) is negligible, because the matrices $\boldsymbol{A}_n$ are very small and remain constant. The trapezoidal rule approximation of (2.31) is

$$\left(I - \frac{\Delta t}{2}\boldsymbol{A}_n\right)\boldsymbol{\psi}^E_{nm}(t_{k+1/2}) = \left(I + \frac{\Delta t}{2}\boldsymbol{A}_n\right)\boldsymbol{\psi}^E_{nm}(t_{k-1/2}) + \Delta t\left(\boldsymbol{E}^k|_{R-\Delta r/2}, \boldsymbol{V}_{nm}\right)\boldsymbol{e}_n, \quad (3.1)$$

where $\boldsymbol{E}^k$ at $r = R - \Delta r/2$ is the average of $\boldsymbol{E}^k$ at $r = R - \Delta r$ and $r = R$. The trapezoidal rule approximation of (2.32) is

$$\left(I - \frac{\Delta t}{2}\boldsymbol{A}_n\right)\boldsymbol{\psi}^H_{nm}(t_{k+1/2}) = \left(I + \frac{\Delta t}{2}\boldsymbol{A}_n\right)\boldsymbol{\psi}^H_{nm}(t_{k-1/2}) + \frac{\Delta t}{2}\left(\boldsymbol{H}^{k-1/2}|_{R-\Delta r/2} + \boldsymbol{H}^{k+1/2}|_{R-\Delta r/2}, \boldsymbol{V}_{nm}\right)\boldsymbol{e}_n. \quad (3.2)$$

The complete algorithm proceeds as follows:

0. Initialize $\boldsymbol{E}$ at $t = 0$ and $\boldsymbol{H}$ at $t = \Delta t/2$, and set $\boldsymbol{\psi}^E_{nm} = 0$ and $\boldsymbol{\psi}^H_{nm} = 0$ at $t = \Delta t/2$.
1. Compute $\boldsymbol{E}$ at $t_k = t_{k-1} + \Delta t$ at all inner points of Ω using (2.1).
2. Compute $\boldsymbol{E}^{\tan}$ at t_k and $r = R$ using (2.30) applied at $r = R - \Delta r/2$ and $t_{k-1/2} = t_{k-1} + \Delta t/2$.
3. Compute $\boldsymbol{H}$ at $t_{k+1/2}$ using (2.1).
4. Compute $\boldsymbol{\psi}^E_{nm}$ and $\boldsymbol{\psi}^H_{nm}$ at $t_{k+1/2}$ using (3.1) and (3.2), respectively, and return to 1.

Although the artificial boundary must be spherical, the boundary condition is not tied to any coordinate system, and the grid used inside Ω can be arbitrary. See [17] for how to fit a Cartesian mesh to curvilinear coordinates, or [18] for a structured spherical mesh without singularities.

4. ALTERNATIVE FORMULATIONS

We shall now show how to reduce the work involved in forming the inner products in (2.31)–(2.32). This slight modification will also render the boundary condition particularly useful when the problem is formulated in terms of $\boldsymbol{E}$ (or $\boldsymbol{H}$) only and the vector wave equation (2.2) is used in Ω. Next, we shall present an alternative formulation of the boundary condition, which fits naturally into the weak formulation of the problem, and therefore is ideally suited for the finite element method.

The work involved in forming the inner products with $\boldsymbol{E}^{\tan}$ and $\boldsymbol{H}^{\tan}$ in (2.31)–(2.32) can be reduced. Indeed, if we compute $\hat{\boldsymbol{r}} \cdot \partial_t \boldsymbol{E}_{nm}$ in (2.12) and use (2.7), we see that

$$\hat{\boldsymbol{r}} \cdot \frac{\partial \boldsymbol{E}_{nm}}{\partial t} = -\frac{\sqrt{n(n+1)}}{\varepsilon R} g_{nm} Y_{nm}, \quad r = R. \quad (4.1)$$

By taking the inner product of (4.1) with Y_{nm} we get

$$g_{nm} = -\frac{\varepsilon R}{\sqrt{n(n+1)}}\left(\hat{\boldsymbol{r}}\cdot\frac{\partial \boldsymbol{E}}{\partial t}, Y_{nm}\right), \quad r = R. \tag{4.2}$$

Therefore, we can compute g_{nm} with one scalar inner product. The time derivative in (4.2) can be replaced by *tangential* spatial derivatives by using (2.1) to yield

$$g_{nm} = -\frac{R}{\sqrt{n(n+1)}}(\hat{\boldsymbol{r}}\cdot\nabla\times\boldsymbol{H}, Y_{nm}), \quad r = R. \tag{4.3}$$

Similarly,

$$f_{nm} = \frac{\mu R}{\sqrt{n(n+1)}}\left(\hat{\boldsymbol{r}}\cdot\frac{\partial \boldsymbol{H}}{\partial t}, Y_{nm}\right), \quad r = R, \tag{4.4}$$

$$= -\frac{R}{\sqrt{n(n+1)}}(\hat{\boldsymbol{r}}\cdot\nabla\times\boldsymbol{E}, Y_{nm}), \quad r = R. \tag{4.5}$$

Equations (4.2) and (4.5) are particularly useful when the vector wave equation is used inside Ω and the problem is written in terms of $\boldsymbol{E}$ (or $\boldsymbol{H}$) only. Then the boundary condition (2.30) can be used, with $(\boldsymbol{H}, \boldsymbol{V}_{nm})$ in (2.32) replaced by the right side of (4.2). Thus applying the boundary condition at $\mathcal{B}$ involves only tangential derivatives of $\boldsymbol{E}$.

The boundary conditions (2.29) and (2.30) fit naturally into finite difference methods. We shall now show how they can be reformulated easily to accommodate finite element methods. To derive the weak form of Maxwell's equations, both Eqs. (2.1) are multiplied by test functions and integrated over Ω. Integration by parts then introduces terms of the form $\hat{\boldsymbol{r}}\times\boldsymbol{E}$ or $\hat{\boldsymbol{r}}\times\boldsymbol{H}$ over $\mathcal{B}$ (see [19, 20]), which we shall now express in terms of known quantities.

We begin by introducing

$$\boldsymbol{\Psi}^E_{nm}(t) = \int_0^t \boldsymbol{\psi}^E_{nm}(s)\,ds, \quad \boldsymbol{\Psi}^H_{nm}(t) = \int_0^t \boldsymbol{\psi}^H_{nm}(s)\,ds. \tag{4.6}$$

Therefore, $\boldsymbol{\Psi}^E_{nm}$ and $\boldsymbol{\Psi}^H_{nm}$ satisfy the same ordinary differential equations as $\boldsymbol{\psi}^E_{nm}$ and $\boldsymbol{\psi}^H_{nm}$, but with f_{nm} and g_{nm} replaced by their time integrals. By integrating (4.2) and (4.5) in time, we conclude that $\boldsymbol{\Psi}^E_{nm}$ is the solution of

$$\frac{1}{c}\frac{d}{dt}\boldsymbol{\Psi}^E_{nm}(t) = \boldsymbol{A}_n\boldsymbol{\Psi}^E_{nm}(t) + \frac{\mu R}{\sqrt{n(n+1)}}(\hat{\boldsymbol{r}}\cdot\boldsymbol{H}|_{r=R}, Y_{nm})\,\boldsymbol{e}_n, \quad \boldsymbol{\Psi}^E_{nm}(0) = 0, \tag{4.7}$$

and that $\boldsymbol{\Psi}^H_{nm}$ is the solution of

$$\frac{1}{c}\frac{d}{dt}\boldsymbol{\Psi}^H_{nm}(t) = \boldsymbol{A}_n\boldsymbol{\Psi}^H_{nm}(t) - \frac{\varepsilon R}{\sqrt{n(n+1)}}(\hat{\boldsymbol{r}}\cdot\boldsymbol{E}|_{r=R}, Y_{nm})\,\boldsymbol{e}_n, \quad \boldsymbol{\Psi}^H_{nm}(0) = 0. \tag{4.8}$$

We note that the inner products in (4.7) and (4.8) involve only scalar inner products with the radial components of $\boldsymbol{E}$ and $\boldsymbol{H}$. Next, we integrate (2.29), and (2.30) with respect to time. The right sides remain the same, with $\boldsymbol{\psi}^E_{nm}$ and $\boldsymbol{\psi}^H_{nm}$ replaced by $\boldsymbol{\Psi}^E_{nm}$ and $\boldsymbol{\Psi}^H_{nm}$. The left

sides can be reformulated easily using (2.1), which leads to the alternative formulation of the nonreflecting boundary condition at $r = R$:

$$\varepsilon \hat{\boldsymbol{r}} \times \boldsymbol{E} - \frac{1}{c}\boldsymbol{H}^{\tan} = \sqrt{\frac{\varepsilon}{\mu}}\frac{1}{R}\sum_{n\geq 1}\sum_{|m|\leq n} \boldsymbol{d}_n \cdot \boldsymbol{\Psi}^E_{nm}(t)\boldsymbol{U}_{nm} + \frac{1}{R}\sum_{n\geq 1}\sum_{|m|\leq n} \boldsymbol{d}_n \cdot \boldsymbol{\Psi}^H_{nm}(t)\boldsymbol{V}_{nm}, \quad r = R, \tag{4.9}$$

$$\mu \hat{\boldsymbol{r}} \times \boldsymbol{H} + \frac{1}{c}\boldsymbol{E}^{\tan} = -\frac{1}{R}\sum_{n\geq 1}\sum_{|m|\leq n} \boldsymbol{d}_n \cdot \boldsymbol{\Psi}^E_{nm}(t)\boldsymbol{V}_{nm} + \sqrt{\frac{\mu}{\varepsilon}}\frac{1}{R}\sum_{n\geq 1}\sum_{|m|\leq n} \boldsymbol{d}_n \cdot \boldsymbol{\Psi}^H_{nm}(t)\boldsymbol{U}_{nm}, \quad r = R. \tag{4.10}$$

Either (4.9) or (4.10) can be used in the weak formulation of the problem inside Ω. Since they do not involve any derivatives of $\boldsymbol{E}$ or $\boldsymbol{H}$, they are particularly easy to combine with a numerical method. When the method of lines is used, the vector of unknowns involves the values of $\boldsymbol{E}$ and $\boldsymbol{H}$ at the interior nodes, together with the unknown functions $\boldsymbol{\Psi}^E_{nm}(t)$ and $\boldsymbol{\Psi}^H_{nm}(t)$, which are advanced concurrently using (4.7) and (4.8). It is quite remarkable that the two scalar quantities $\hat{\boldsymbol{r}} \cdot \boldsymbol{E}$ and $\hat{\boldsymbol{r}} \cdot \boldsymbol{H}$ suffice to impose the nonreflecting boundary condition.

5. HIGHER ORDER BOUNDARY CONDITIONS

In practice, the infinite sums in (2.29) and (2.30) must be truncated at some finite value N. For the modes $n > N$, the truncated boundary condition for $\boldsymbol{H}$ reduces to

$$\hat{\boldsymbol{r}} \times \nabla \times \boldsymbol{H} - \frac{1}{c}\frac{\partial \boldsymbol{H}^{\tan}}{\partial t} = 0. \tag{5.1}$$

This is the time-dependent counterpart of the first-order approximate boundary condition derived by Peterson [4], which annihilates the leading term in the large distance expansion of the electromagnetic field [21]. The truncation at N introduces an error $O(R^{-3})$ in modes with $n > N$. To reduce that error, without affecting the modes $n \leq N$, we transform the second-order Peterson condition [4] to the time domain to obtain

$$\left\{\hat{\boldsymbol{r}} \times (\nabla\times) - \frac{1}{c}\frac{\partial}{\partial t} - \frac{2}{r}\right\}\left\{\hat{\boldsymbol{r}} \times \nabla \times \boldsymbol{H} - \frac{1}{c}\frac{\partial \boldsymbol{H}^{\tan}}{\partial t}\right\} = 0, \quad r = R. \tag{5.2}$$

The error in (5.2) is $O(R^{-5})$, which is smaller than the error $O(R^{-3})$ in (5.1) for $R > 1$.

To take advantage of this smaller error, we apply the operator $(\hat{\boldsymbol{r}} \times (\nabla\times) - c^{-1}\partial_t - 2/r)$ to both sides of (2.29) and (2.30). The resulting boundary conditions are still exact, but when truncated at $n = N$ they yield (5.2) for the modes with $n > N$, with error $O(R^{-5})$. We shall carry out the calculations for the component $\boldsymbol{H}_{nm}$, which satisfies (2.18). To do so we derive the following formula, similar to (2.8), which holds for any $f(r)$:

$$\hat{\boldsymbol{r}} \times \nabla \times (f(r)\boldsymbol{U}_{nm}) = -\frac{1}{r}\frac{\partial (r f(r))}{\partial r}\boldsymbol{U}_{nm}. \tag{5.3}$$

By using (2.8) and (5.3) we obtain from (2.18)

$$\left\{\hat{\boldsymbol{r}}\times(\nabla\times)-\frac{1}{c}\frac{\partial}{\partial t}-\frac{2}{r}\right\}\left\{\hat{\boldsymbol{r}}\times\nabla\times\boldsymbol{H}_{nm}-\frac{1}{c}\frac{\partial\boldsymbol{H}_{nm}^{\tan}}{\partial t}\right\}$$
$$=\sqrt{\frac{\varepsilon}{\mu}}\frac{1}{r}\left(\frac{\partial}{\partial r}+\frac{1}{c}\frac{\partial}{\partial t}+\frac{2}{r}\right)\left(\frac{\partial}{\partial r}+\frac{1}{c}\frac{\partial}{\partial t}\right)[r f_{nm}]\boldsymbol{U}_{nm}$$
$$+\frac{1}{r}\left(\frac{\partial}{\partial r}+\frac{1}{c}\frac{\partial}{\partial t}+\frac{2}{r}\right)\left(\frac{\partial}{\partial r}+\frac{1}{c}\frac{\partial}{\partial t}\right)[r g_{nm}]\boldsymbol{V}_{nm}. \tag{5.4}$$

In [2, Section 5] it was shown that the exact second-order boundary condition for $f_{nm}(r,t)$ is

$$\left(\frac{\partial}{\partial r}+\frac{1}{c}\frac{\partial}{\partial t}+\frac{2}{r}\right)\left(\frac{\partial}{\partial r}+\frac{1}{c}\frac{\partial}{\partial t}\right)[r f_{nm}]=\tilde{\boldsymbol{d}}_n\cdot\boldsymbol{\psi}_{nm}^E(t),\quad r=R, \tag{5.5}$$

where the vector functions $\boldsymbol{\psi}_{nm}^E(t)$ satisfy (2.21), and the constant vectors $\tilde{\boldsymbol{d}}_n=\{\tilde{d}_n^j\}$ are defined by

$$\tilde{d}_n^j=\frac{n(n+1)j(j-1)}{2R^j},\quad j=1,\ldots,n. \tag{5.6}$$

We note that $\tilde{d}_1^1=0$ and, hence, that the terms with $n=1$ in the sums vanish. Therefore, the second-order absorbing boundary condition (5.2) is exact for the multipoles with $n=1$.

We use (5.5) in (5.4), set $r=R$, and finally sum over n and m to obtain the exact non-reflecting boundary condition. The exact second-order boundary condition for the magnetic field at $r=R$ is

$$\left\{\hat{\boldsymbol{r}}\times(\nabla\times)-\frac{1}{c}\frac{\partial}{\partial t}-\frac{2}{R}\right\}\left\{\hat{\boldsymbol{r}}\times\nabla\times\boldsymbol{H}-\frac{1}{c}\frac{\partial\boldsymbol{H}_{nm}^{\tan}}{\partial t}\right\}$$
$$=\sqrt{\frac{\varepsilon}{\mu}}\frac{1}{R^2}\sum_{n\geq2}\sum_{|m|\leq n}\tilde{\boldsymbol{d}}_n\cdot\boldsymbol{\psi}_{nm}^E(t)\boldsymbol{U}_{nm}+\frac{1}{R^2}\sum_{n\geq2}\sum_{|m|\leq n}\tilde{\boldsymbol{d}}_n\cdot\boldsymbol{\psi}_{nm}^H(t)\boldsymbol{V}_{nm}. \tag{5.7}$$

The exact second-order boundary condition for the electric field at $r=R$ is

$$\left\{\hat{\boldsymbol{r}}\times(\nabla\times)-\frac{1}{c}\frac{\partial}{\partial t}-\frac{2}{R}\right\}\left\{\hat{\boldsymbol{r}}\times\nabla\times\boldsymbol{E}-\frac{1}{c}\frac{\partial E^{\tan}}{\partial t}\right\}$$
$$=\frac{1}{R^2}\sum_{n\geq2}\sum_{|m|\leq n}\tilde{\boldsymbol{d}}_n\cdot\boldsymbol{\psi}_{nm}^E(t)\boldsymbol{V}_{nm}-\sqrt{\frac{\mu}{\varepsilon}}\frac{1}{R^2}\sum_{n\geq2}\sum_{|m|\leq n}\tilde{\boldsymbol{d}}_n\cdot\boldsymbol{\psi}_{nm}^H(t)\boldsymbol{U}_{nm}. \tag{5.8}$$

Here the vector functions $\boldsymbol{\psi}_{nm}^E(t)$ and $\boldsymbol{\psi}_{nm}^H(t)$ satisfy the same ordinary differential equations (2.31) and (2.32). The constant vectors $\tilde{\boldsymbol{d}}_n$ are given by (5.6), $\boldsymbol{e}_n$ by (2.24), and the constant matrices $\boldsymbol{A}_n$ by (2.22).

The same procedure can be adapted easily to accommodate modifications of (5.2), which may possess certain practical advantages [22]. If the radius of $\mathcal{B}$ and the temporal frequency remain fixed, the error introduced at $\mathcal{B}$ by imposing (5.2) on the multipole $\boldsymbol{H}_{nm}$ increases with increasing n [22].

6. NUMERICAL RESULTS

We shall now combine the finite difference method with the nonreflecting boundary condition, as described in Section 3, and apply it to a model problem for which the exact solution is known. In Ref. [2], we have presented examples which show the accuracy of this method for the scalar wave equation, and we have discussed storage requirements and other computational issues.

We consider an off-centered radiating electric dipole located at $S = (0, 0, z_0)$, $z_0 > 0$, at distance z_0 from the origin. The dipole is aligned along z, so that its moment points along the positive z-axis. Its time dependence, shown in Fig. 1, is a Gaussian pulse centered at $t = t_0$:

$$P(t) = \begin{cases} 0, & t < 0, \\ \alpha e^{-(t-t_0)^2/\sigma^2}, & 0 \le t \le 2t_0, \\ 0, & t > 2t_0. \end{cases} \tag{6.1}$$

We set $\alpha = 10^{-9}$ and choose σ so that $P(t)$ is equal to machine precision at $t = 0$ and $t = 2t_0$.

Since this problem is symmetric about the z-axis, the electromagnetic field has only three nonvanishing components: $\boldsymbol{E}(r, \theta, t) = E^r \hat{\boldsymbol{r}} + E^\theta \hat{\boldsymbol{\vartheta}}$ and $\boldsymbol{H}(r, \theta, t) = H^\phi \hat{\boldsymbol{\phi}}$. Furthermore, the exact solution can be found in [24, p. 152]. We impose the tangential component E^θ of

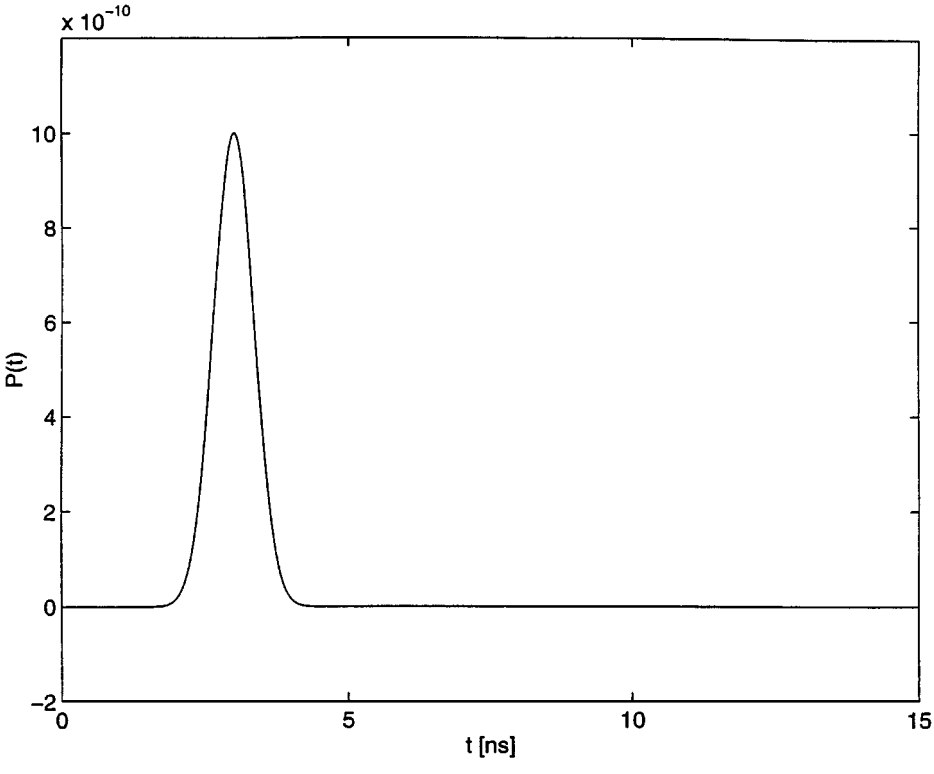

FIG. 1. The time dependence $P(t)$ of the dipole source.

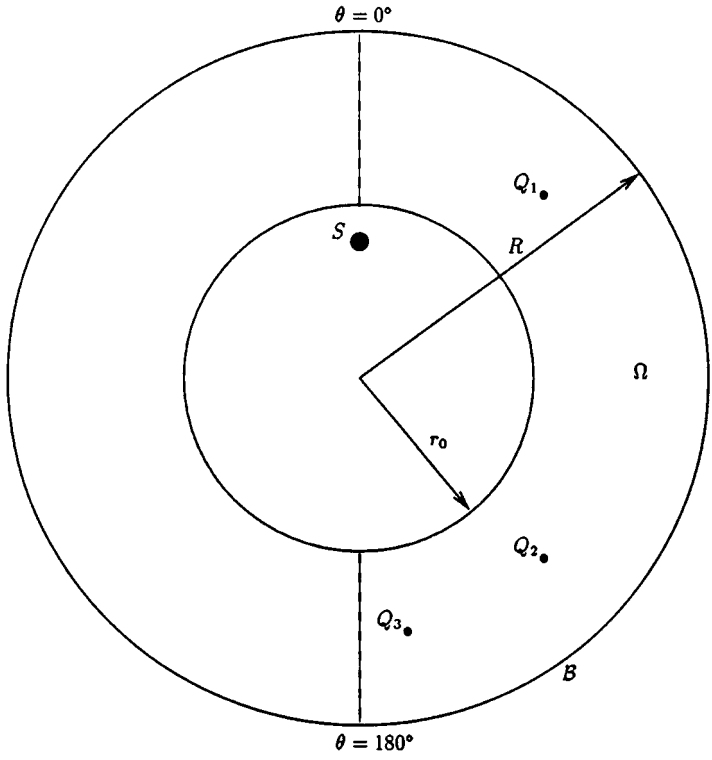

FIG. 2. The computational domain Ω is shown drawn to scale, with $r_0 = 0.5$ [m] and $R = 1$ [m]. The dipole source is located at $S = (0, 0, z_0)$, with $z_0 = 0.4$ [m].

the exact solution as a boundary condition at $r = r_0$ and calculate its propagation outwards up to the artificial boundary $r = R$. Because of the inherent symmetry, the computational domain Ω can be reduced to the two-dimensional region $r_0 \le r \le R, 0 \le \theta \le \pi$, shown in Fig. 2. Inside Ω we use polar coordinates and a uniform mesh in r and θ. The Yee algorithm in polar coordinates is described in [23] or [15, pp. 378–381]. We set $r_0 = 0.5$ [m], $R = 1$ [m], $z_0 = 0.4$ [m], $c = 2.998 \times 10^8$ [m/s], and $t_0 = 3$ [ns].

We shall compare the numerical solution using (2.30), where the sums are truncated at N, with that obtained using the first-order condition (5.1). We denote the former by NBC(N), where N indicates the upper limit in the sums, and the latter by P1 to acknowledge [4]. We recall that P1 is identical to NBC(0). The boundary condition (2.30) is implemented as described in Section 3, albeit due to the radial symmetry, $\psi^E_{nm}(t)$ is identically zero.

In Fig. 3, we check the accuracy of our numerical method. The maximal error in the L_2-norm over the time interval [0, 15], nanoseconds is shown versus the mesh parameter $h = \Delta r$, for the following sequence of meshes: 20×120, 30×180, 40×240, 60×360, and 80×480. We observe the expected second-order convergence of the full scheme using NBC(20) as the mesh is refined. This indicates that setting $N = 20$ ensures that the error introduced at the artificial boundary is smaller than that of the numerical scheme. However, the error in the numerical solution obtained with P1 does not decrease as the mesh is refined, indicating that the error introduced by using P1 dominates the computation. Indeed, the numerical solution does not converge to the solution of the original problem, but instead converges to the solution of a different problem with P1 imposed at $\mathcal{B}$. When NBC(N)

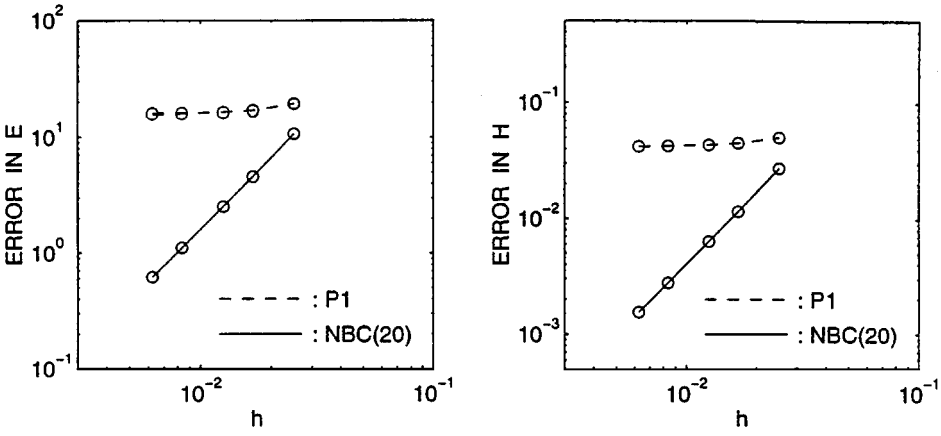

FIG. 3. The maximal error in the L_2 norm over the time interval [0, 15] nanoseconds is shown versus the mesh parameter $h = \Delta r$: $\boldsymbol{E}^h$ (left) and $\boldsymbol{H}^h$ (right).

is implemented numerically, $N = N(h)$ can be chosen high enough to reduce the error introduced at $\mathcal{B}$ below the discretization error of the numerical method inside Ω, without moving the artificial boundary farther away from the scatterer. With $N(h)$ chosen in this way, the numerical method will converge to the correct solution as h tends to zero.

Next, we shall compare the numerical solutions, obtained using P1 and NBC(20), with the exact solution at three different locations well inside Ω at $r = 0.75$ [m]: Q_1 ($\theta = 45^\circ$), Q_2 ($\theta = 135^\circ$), and Q_3 ($\theta = 170^\circ$). The inner and outer radii remain at their current locations $r_0 = 0.5$ [m], and $R = 1$ [m], and we choose a 60×360 mesh inside Ω.

In Fig. 4, the ϕ-component of the magnetic field is shown at the first location Q_1. The numerical solution obtained with NBC(20) is hardly distinguishable from the exact solution. While the relative error due to the P1 boundary condition is only a few percent, this seemingly accurate behavior is deceptive.

Indeed these *locally* small reflections travel back into the computational domain and contaminate the solution everywhere inside Ω, in particular in regions where the solution is of much lesser magnitude. To demonstrate this point, we select the next location farther from the source at Q_2, where the electromagnetic field is much weaker. The ϕ-component of the magnetic field at Q_2 is shown in Fig. 5, and again it agrees completely with the numerical solution obtained using NBC(20). The solution obtained using P1 agrees with the exact solution for a finite time. It then diverges from it, as the spurious reflection due to the imposition of P1 reaches this location.

This effect is even more dramatic if we choose a location close to the south pole at Q_3. In Fig. 6, the ϕ-component of the magnetic field is shown at Q_3. Here the spurious reflection due to the P1 boundary condition is *larger than the original signal*. The solution obtained using NBC(20) agrees well with the exact solution.

Finally, we set $R = 0.6$ [m] to study the performance of the boundary conditions as the outer boundary is moved closer to the inner one. The mesh size remains identical, so that the mesh has 12×360 points. In Fig. 7, the r-component of the electric field is shown below the south pole of the inner sphere at the severe test location $\theta = 180^\circ$ and $r = 0.55$ [m]. Again, the numerical solution obtained using NBC(20) agrees with the exact solution; this demonstrates the robustness of the exact boundary condition with respect to the location

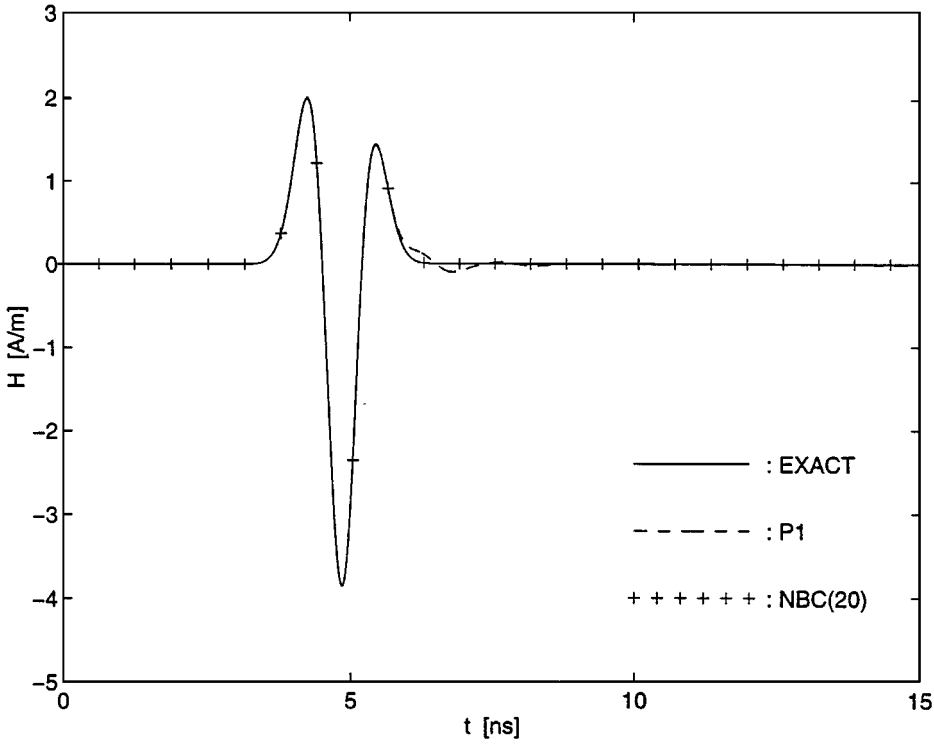

FIG. 4. The numerical solutions for H^{ϕ}, computed using the boundary conditions P1 and NBC(20), are compared with the exact solution at Q_1.

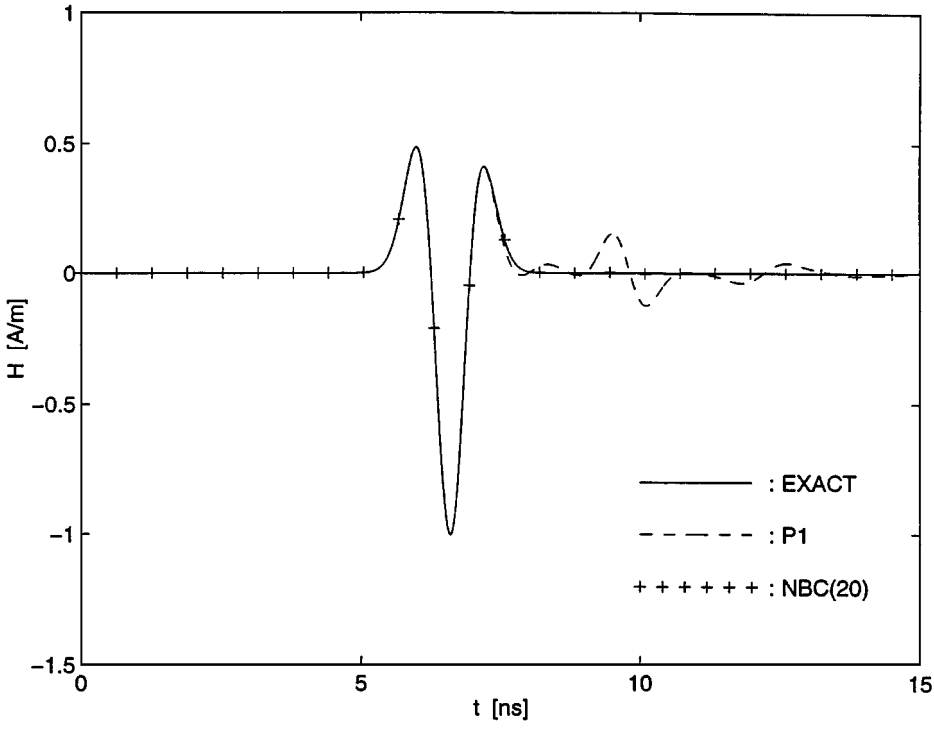

FIG. 5. The numerical solutions for H^{ϕ}, computed using the boundary conditions P1 and NBC(20), are compared with the exact solution at Q_2.

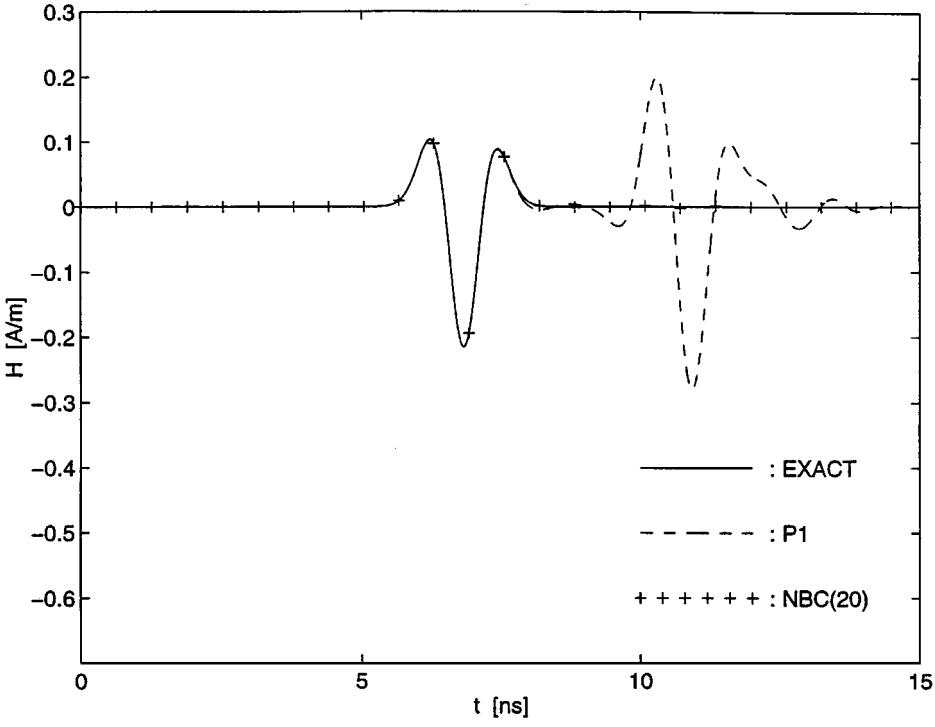

FIG. 6. The numerical solutions for H^{ϕ}, computed using the boundary conditions P1 and NBC(20), are compared with the exact solution at Q_3.

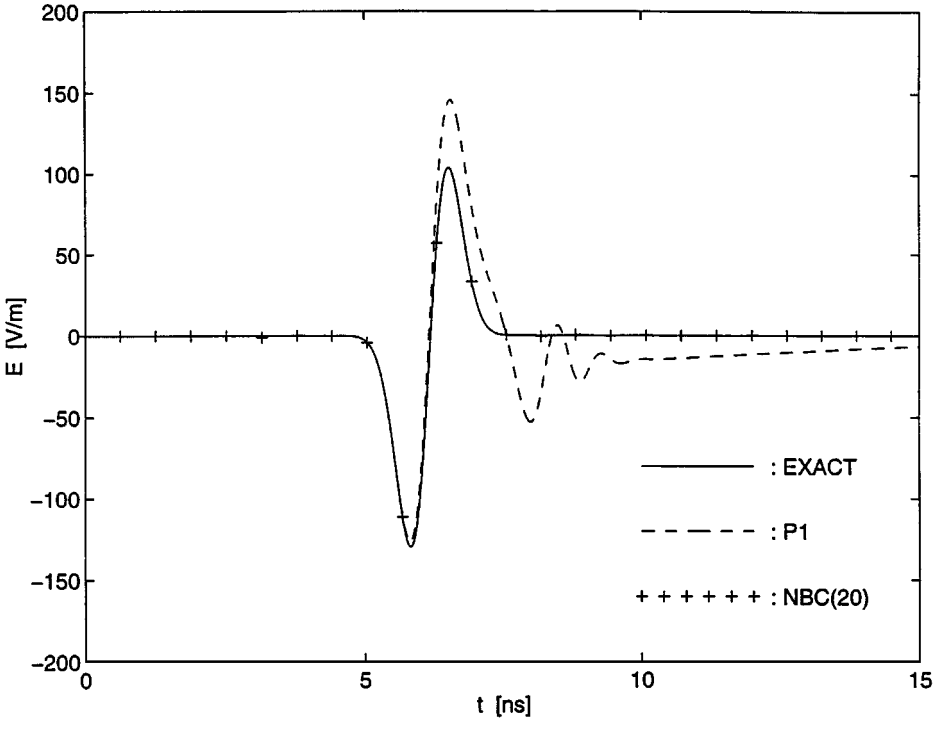

FIG. 7. The numerical solutions for E^{r}, computed using the boundary conditions P1 and NBC(20) at $R = 0.6$ [m], are compared with the exact solution at $r = 0.55$ [m], $\theta = 180^{\circ}$.

of the artificial boundary. The numerical solution obtained with P1 agrees with the exact solution for a short time. It then strongly overshoots, oscillates a few times, and slowly starts to approach zero. This suggests that using the exact nonreflecting boundary condition may be useful even in calculations where the transient behavior is of no interest, since the numerical solution may reach the final steady state much faster.

7. CONCLUSION

We have, derived an exact boundary condition for the time-dependent Maxwell equations in three space dimensions. It holds at the surface of a sphere and is local in time. It is given by (2.29) and (2.30) and fits naturally into standard finite difference methods. An alternative formulation, more suitable for finite element methods, is given by (4.9) and (4.10). Both boundary conditions require little extra storage and computer time and can reduce the error introduced by the artificial boundary below the discretization error due to the numerical method, regardless of the radius of the outer boundary. For fields which contain modes with $n > N$, greater accuracy is provided by the higher order boundary conditions of Section 5.

REFERENCES

1. M. J. Grote and J. B. Keller, *SIAM J. Appl. Math.* **55**, 280 (1995).
2. M. J. Grote and J. B. Keller, *J. Comput. Phys.* **127**, 52 (1996).
3. G. Mur, *IEEE Trans. Electromagn. Compat.* **EMC-23**, 377 (1981).
4. A. F. Peterson, *Microwave Opt. Techn. Lett.* **1**, 62 (1988).
5. B. Engquist and A. Majda, *Math. Comp.* **31**, 629 (1977).
6. A. Bayliss and E. Turkel, *Comm. Pure Appl. Math.* **33**, 707 (1980).
7. J.-P. Bérenger, *J. Comput. Phys.* **114**, 185 (1994).
8. E. L. Lindman, *J. Comput. Phys.* **18**, 66 (1975).
9. C. J. Randall, *Geophysics* **53**, 611 (1988). [*Geophysics* **54**, 1141 (1989)]
10. L. Ting and M. J. Miksis, *J. Acoust. Soc. Amer.* **80**, 1825 (1986).
11. J. De Moerloose and D. De Zutter, *IEEE Trans. Antenn. Propag.* **41**, 890 (1993).
12. D. Colton and R. Kress, *Inverse Acoustic and Electromagnetic Scattering Theory* (Springer Verlag, New York/Berlin, 1992).
13. J. D. Jackson, *Classical Electrodynamics*, 2nd ed. (Wiley, New York, 1975).
14. K. S. Yee, *IEEE Trans. Antennas Propag.* **14**, 302 (1966).
15. K. S. Kunz and R. J. Luebbers, *Finite Difference Time Domain Methods for Electromagnetics* (CRC Press, Boca Raton, FL, 1993).
16. E. Hairer, S. P. Nørsett, and G. Wanner, *Solving Ordinary Differential Equations I* (Springer Verlag, New York/Berlin, 1987).
17. A. Taflove and K. R. Umashankar, *Electromagnetics.* **10**, 105 (1990).
18. C. Ronchi, R. Iacono, and P. S. Paolucci, *J. Comput. Phys.* **124**, 93 (1996).
19. R. L. Lee and N. K. Madsen, *J. Comput. Phys.* **88**, 284 (1990).
20. P. Monk, *SIAM J. Sci. Stat. Comput.* **13**, 1097 (1992).
21. C. H. Wilcox, *Comm. Pure Appl. Math.* **9**, 115 (1956).
22. A. F. Peterson, *IEEE Trans. Antenn. Propag.* **40**, 351 (1992).
23. R. Holland, *IEEE Trans. Nucl. Science* **30**, 4592 (1983).
24. D. S. Jones, *The Theory of Electromagnetism* (Pergamon/Macmillan, New York, 1964).